

Cross section of the process $e^+e^- \rightarrow n\bar{n}$ near the threshold

M. N. Achasov,^{1,2} A. Yu. Barnyakov,^{1,2} E. V. Bedarev,^{1,2} K. I. Beloborodov,^{1,2}
 A. V. Berdyugin,^{1,2} A. G. Bogdanchikov,¹ A. A. Botov,¹ T. V. Dimova,^{1,2}
 V. P. Druzhinin,^{1,2} V. N. Zhabin,^{1,2} Yu. M. Zharinov,¹ L. V. Kardapoltsev,^{1,2}
 A. S. Kasaev,¹ A. A. Kattsin,¹ D. P. Kovrizhin,¹ A. A. Korol,^{1,2}
 A. S. Kupich,^{1,2} A. P. Kryukov,¹ A. P. Lysenko,¹ N. A. Melnikova,¹
 N. Yu. Muchnoi,^{1,2} A. E. Obrazovsky,¹ E. V. Pakhtusova,¹ K. V. Pugachev,^{1,2}
 S. A. Rastigeev,¹ Yu. A. Rogovsky,^{1,2} A. I. Senchenko,¹ S. I. Serednyakov,^{1,2,*}
 Z. K. Silagadze,^{1,2} I. K. Surin,¹ Yu. V. Usov,¹ A. G. Kharlamov,^{1,2}
 D. E. Chistyakov,^{1,2} Yu. M. Shatunov,¹ S. P. Sherstyuk,^{1,2} and D. A. Shtol¹

¹*Budker Institute of Nuclear Physics, SB RAS, Novosibirsk 630090, Russia*

²*Novosibirsk State University, Novosibirsk 630090, Russia*

(Dated:)

The $e^+e^- \rightarrow n\bar{n}$ cross section was measured at center of mass (c.m.) energies from the threshold to 1908 MeV. The experiment to measure the cross section has been carried out at the VEPP-2000 e^+e^- collider in 13 energy points. The SND detector is used to detect the produced neutron-antineutrons ($n\bar{n}$) events. A special time measurement system on the calorimeter was used to select the time-delayed $n\bar{n}$ events. The measured $e^+e^- \rightarrow n\bar{n}$ cross section is 0.4–0.6 nb. The neutron effective timelike form factor in the energy range under study varies from 0.3 to 0.6.

*Electronic address: S.I.Serednyakov@inp.nsk.su

Introduction

The e^+e^- annihilation to neutron-antineutron pairs depends on two form factors - electric G_E and magnetic G_M :

$$\frac{d\sigma}{d\Omega} = \frac{\alpha^2\beta}{4s} \left[|G_M(s)|^2(1 + \cos^2\theta) + \frac{1}{\gamma^2}|G_E(s)|^2 \sin^2\theta \right], \quad (1)$$

where α is the fine structure constant, $s = 4E_b^2 = E^2$, where E_b is the beam energy and E is the center-of-mass (c.m.) energy, $\beta = \sqrt{1 - 4m_n^2/s}$, $\gamma = E_b/m_n$, m_n is the neutron mass and θ is the antineutron production polar angle. The total cross section has the following form:

$$\sigma(s) = \frac{4\pi\alpha^2\beta}{3s} \left(1 + \frac{1}{2\gamma^2}\right) |F(s)|^2, \quad (2)$$

where the effective form factor $F(s)$ is introduced:

$$|F(s)|^2 = \frac{2\gamma^2|G_M(s)|^2 + |G_E(s)|^2}{2\gamma^2 + 1}. \quad (3)$$

The $|G_E/G_M|$ ratio can be extracted from the analysis of the measured $\cos\theta$ distribution in Eq. (1). At the threshold $|G_E| = |G_M|$.

The $e^+e^- \rightarrow n\bar{n}$ process in the threshold region was first observed in the FENICE [1] and DM2 [2] experiments. Much more accurate measurements are being carried out at the VEPP-2000 e^+e^- collider with the SND detector [3], [4]. At the energy above 2 GeV new data have been obtained by the BESIII [5]. In this work we present the results of measurements at the beam energy range ~ 15 MeV above the nucleon threshold with a scanning step close to the beam energy spread.

I. COLLIDER, DETECTOR, EXPERIMENT

VEPP-2000 is the e^+e^- collider [6] operating in the c.m. energy range from the hadron threshold ($E=280$ MeV) up to 2 GeV. The collider luminosity above the nucleon threshold is of order of $5 \times 10^{31} \text{ cm}^{-2}\text{s}^{-1}$. There are two collider detectors at VEPP-2000: SND and CMD-3.

SND (Spherical Neutral Detector) [7] is a non-magnetic detector, including a tracking system, a spherical NaI(Tl) electromagnetic calorimeter (EMC) and a muon detector (Fig.1).

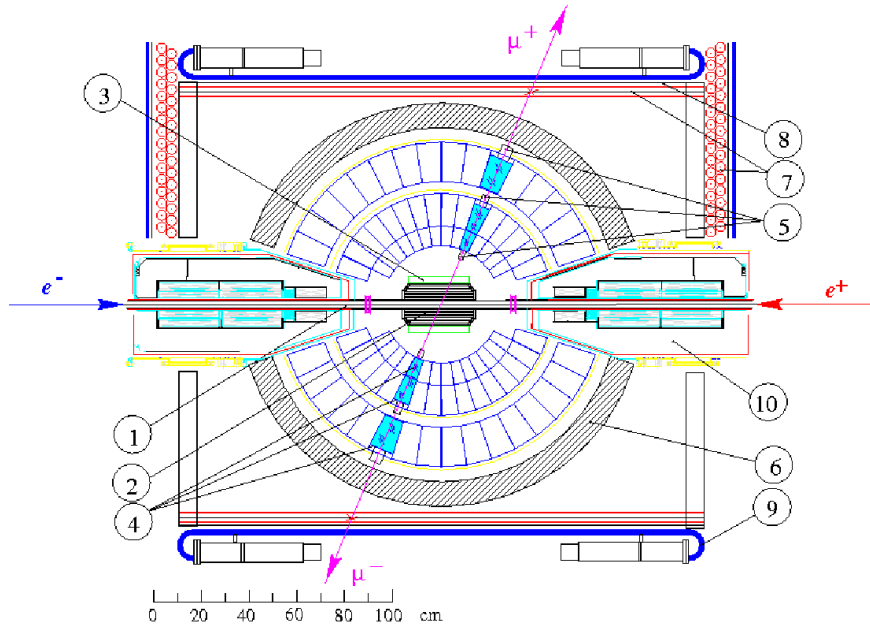


FIG. 1: SND detector, section along the beams: (1) beam pipe, (2) tracking system, (3) aerogel Cherenkov counters, (4) NaI (Tl) crystals, (5) vacuum phototriodes, (6) iron absorber, (7) proportional tubes, (8) iron absorber, (9) scintillation counters, (10) VEPP-2000 focusing solenoids.

The EMC is the main part of the SND used in the $n\bar{n}$ analysis. The thickness of EMC is 34.7 cm (13.4 radiation length). The antineutron annihilation length in NaI(Tl) varies with energy from several cm close to the $n\bar{n}$ threshold to ~ 15 cm at the maximum energy [8], so nearly all produced antineutrons are absorbed in the detector.

In $n\bar{n}$ analysis the EMC is used to measure the event arrival time relative to the moment of beam collision. For this on each of the 1640 EMC counters a special flash ADC module [9], measuring the signal waveform, is installed. When fitting the flash ADC output waveform with a pre-set function, the time and amplitude of the signal in the counters with more than 5 MeV energy, are calculated. The event time is calculated as the EMC counters energy weighted average time [10]. The time resolution obtained with data $e^+e^- \rightarrow \gamma\gamma$ events is about 0.8 ns. This value is greater than Monte Carlo resolution of 0.3 ns due to the finite time resolution of the timing system. So we convolve the MC $\gamma\gamma$ time spectrum with a Gaussian with $\sigma_{\gamma\gamma} = 0.8$ ns. For $e^+e^- \rightarrow n\bar{n}$ events the convolution is done with $\sigma_{nn} = 1.5-2$ ns depending on the energy.

This article presents the $n\bar{n}$ analysis results of data with the integrated luminosity of about 100 pb^{-1} , collected in the c.m. energy range from the threshold to 1.908 GeV in 13

energy points. The value of the lowest beam energy (939.59 MeV) is just at the process threshold. That's why here due to the beam energy spread only in half of e^+e^- collisions the $n\bar{n}$ pairs are produced. Taking this into account the average beam energy at this point increases to the value of 939.93 MeV, which is above the threshold by 0.36 MeV. The effective luminosity at this point will be two times lower than the nominal. The energy values and luminosity at all points are given in the Table I. Our measurement is the first so close to the $n\bar{n}$ threshold.

II. EVENT SELECTION

Antineutron from the $n\bar{n}$ pair in most cases annihilates, producing pions, nucleons, photons and other particles, which deposit up to 2 GeV in EMC. The neutron from the $n\bar{n}$ pair release a small signal in EMC, which is poorly visible against the background of a strong \bar{n} annihilation signal, so it is not taken into account. The $n\bar{n}$ events are reconstructed as multiphoton events. The antineutron production angle is defined by the direction of the total event momentum $P = \sum_i E_i n_i$, where the summation is carried out over the calorimeter crystals, E_i is the crystal energy, n_i is the unit vector. Projections of the vector P onto the direction along and across the beams define the polar and azimuthal antineutron angles. Some of the $n\bar{n}$ events are accompanied by non-beam tracks, which arise during antineutron annihilation in the detector material.

Main features of $n\bar{n}$ events, in contrast to ordinary e^+e^- annihilation events, are absence of charged tracks and photons from the collision region and a strong imbalance in the event momentum. Another feature is the presence of a significant cosmic background events, having a signature similar to $n\bar{n}$ events and comparable to or exceeding the intensity of the $n\bar{n}$ events. There is also the problem of a large background from beams of electrons and positrons in the collider. Based on these specific features of the $e^+e^- \rightarrow n\bar{n}$ process, we have developed the following selection conditions:

- 1 - no charged tracks from the interaction region is found in an event ($n_{ch}=0$),
- 2 - the event momentum must be significantly unbalanced ($P > 0.4E_{EMC}$), what suppress the e^+e^- annihilation background,
- 3 - the transverse EMC energy profile of the found most energetic photon in an event should be broader than that expected for the electromagnetic shower : $L_\gamma > -2.5$, where L_γ

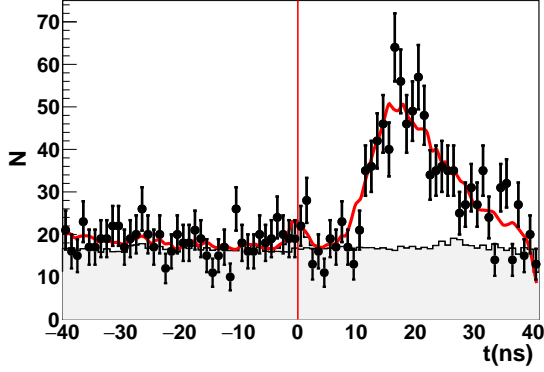


FIG. 2: The time distribution of selected data events at $E_b = 941$ MeV. The solid line (red) is the result of the fit described in the text. Vertical line at $t=0$ shows the position of the beam background.

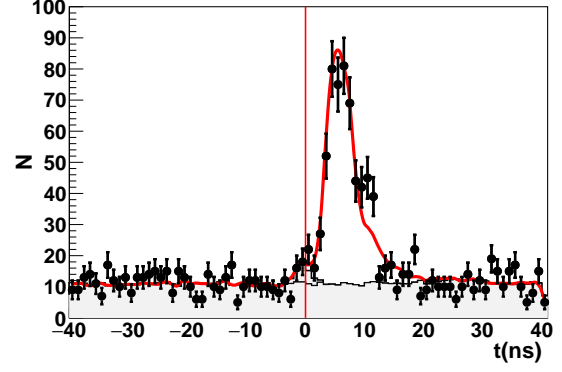


FIG. 3: The time distribution of selected data events at $E_b = 952$ MeV. The solid line (red) is the result of the fit described in the text. Vertical line at $t=0$ shows the position of the beam background.

is the logarithmic parameter, describing the width of the transverse energy profile in EMC [11],

4 - the veto of external muon detector is required,

5 - the events with a cosmic-ray track in EMC, defined as a chain of crystals along a straight line, are rejected,

6 - an additional suppression of cosmic background, that have passed through the muon veto, is carried out by a special parameter (shcosm), that approximates the shape of energy deposition in the calorimeter in the form of ellipsoid [3]. Further, a condition on this parameter is set ($shcosm > 0.4$), which leads to the suppression of cosmic background. Basically, these are cosmic showers in EMC,

7 - the EMC total energy deposition cut is taken to be $E_{EMC} > E_b$, where E_b is the beam energy. Such a cut reduces the $n\bar{n}$ detection efficiency by $\sim 20\%$, but almost completely removes the beam background.

In general, the conditions listed above are similar to those used in our previous works on the $e^+e^- \rightarrow n\bar{n}$ analyses [3], [4]. After imposing the described selection conditions, we have about 400 events/ pb^{-1} left for further analysis.

III. ANALYSIS OF MEASURED TIME SPECTRA

Typical time spectra of events selected for analysis are shown in Figs . 2, 3. Three main components are distinguished in the figures shown: a beam and physical background at $t=0$, a cosmic background uniform in time, and to the right a delayed signal from $n\bar{n}$ events, wide in time. The wide shape of the $n\bar{n}$ time spectrum is explained by the spread of the antineutron annihilation point - from the collider vacuum chamber wall at 2 cm from the beam collision area to 70 cm on the back wall of the calorimeter. Respectively, the measured time spectra are fitted by the sum of these three contributions in the following form :

$$F(t) = N_{n\bar{n}}H_{n\bar{n}}(t) + N_{\text{csm}}H_{\text{csm}}(t) + N_{\text{bkg}}H_{\text{bkg}}(t), \quad (4)$$

where $H_{n\bar{n}}$, H_{csm} and H_{bkg} are normalized histograms, describing time spectra for the $n\bar{n}$ signal, cosmic and beam + physical background, respectively. $N_{n\bar{n}}$, N_{csm} , and N_{bkg} are the corresponding event numbers, obtained from subsequent fit. The shape of the beam+physical background time spectrum H_{bkg} is measured at the energies below the $n\bar{n}$ threshold. The cosmic time spectrum H_{csm} is measured with the lower EMC threshold $0.9 \cdot E_b$ in coincidence with the muon system signal. The shape of the $H_{n\bar{n}}$ spectrum is calculated by the MC simulation the $e^+e^- \rightarrow n\bar{n}$ process. But it turned out that the data $n\bar{n}$ time spectrum is insatisfactorily described by MC shape $H_{n\bar{n}}$. The study of the $n\bar{n}$ simulation showed that it contains two types of the first interaction of the antineutron with matter: 1 - antineutron annihilation and 2 - first antineutron scattering and then annihilation. These types have different time spectra, and in the second case the time spectrum is wider and more delayed. Therefore, in Eq.4 the time spectrum $H_{n\bar{n}}$ was represented as the sum of these two contributions, and the fraction of the scattering contribution was a free fit parameter. As a result of fitting Eq.4 with modified $H_{n\bar{n}}$, the agreement between the data and MC in the time shape has improved significantly. The contribution of the first annihilation turned out to be greater in data than in Monte Carlo by 1.5-2 times. The fitting curves in Figs . 2, 3 are modified in this way.

The detection cross section of the beam+physical background $\sigma_{bg} = N_{bg}/L$, where L is integrated luminosity in a given energy, obtained during fitting, is about 5 pb and does not significantly depend on the beam energy. The main contribution into physical part of σ_{bg} comes from the processes with neutral kaons in the final state: $e^+e^- \rightarrow K_S K_L \pi^0$, $K_S K_L \eta$ and similar other. The role of K_L 's as a source of background is important for two

TABLE I: The beam energy (E_b), integrated luminosity (L), number of selected $n\bar{n}$ events ($N_{n\bar{n}}$), the factor taking into account radiative corrections and energy spread ($1 + \delta$), corrected detection efficiency (ε), measured $e^+e^- \rightarrow n\bar{n}$ cross section σ , and neutron effective form factor (F_n). The quoted errors for N , σ are statistical and systematic. For the detection efficiency, the systematic uncertainty is quoted. For F_n , the combined statistical and systematic uncertainty is listed.

N	$E_b(\text{MeV})$	$L(\text{pb})$	$N_{n\bar{n}}$	$1 + \delta$	ε	$\sigma(\text{nb})$	F_n
1	939.9	5.92	250 ± 72	0.602	0.200 ± 0.105	$0.352 \pm 0.101 \pm 0.193$	0.562 ± 0.174
2	940.3	9.14	313 ± 54	0.633	0.121 ± 0.030	$0.447 \pm 0.076 \pm 0.107$	0.555 ± 0.081
3	941.0	9.70	597 ± 41	0.671	0.209 ± 0.023	$0.440 \pm 0.030 \pm 0.049$	0.467 ± 0.031
4	942.0	10.12	680 ± 37	0.702	0.240 ± 0.020	$0.399 \pm 0.023 \pm 0.034$	0.390 ± 0.020
5	943.5	9.81	747 ± 36	0.731	0.216 ± 0.015	$0.483 \pm 0.023 \pm 0.033$	0.382 ± 0.016
6	945.0	11.45	921 ± 38	0.751	0.233 ± 0.022	$0.461 \pm 0.020 \pm 0.044$	0.345 ± 0.018
7	947.5	10.41	947 ± 37	0.776	0.219 ± 0.011	$0.536 \pm 0.022 \pm 0.027$	0.340 ± 0.011
8	948.75	6.42	611 ± 30	0.787	0.213 ± 0.014	$0.567 \pm 0.028 \pm 0.037$	0.337 ± 0.014
9	950.0	5.20	514 ± 29	0.797	0.211 ± 0.016	$0.585 \pm 0.033 \pm 0.044$	0.333 ± 0.016
10	951.0	5.55	522 ± 29	0.804	0.223 ± 0.016	$0.525 \pm 0.029 \pm 0.039$	0.309 ± 0.015
11	952.0	5.26	485 ± 26	0.811	0.224 ± 0.015	$0.507 \pm 0.027 \pm 0.035$	0.298 ± 0.013
12	953.0	5.68	513 ± 28	0.818	0.246 ± 0.017	$0.450 \pm 0.024 \pm 0.032$	0.276 ± 0.012
13	954.0	5.17	540 ± 27	0.824	0.234 ± 0.015	$0.519 \pm 0.027 \pm 0.034$	0.291 ± 0.012

reasons: 1 - some of K_L 's pass through the calorimeter without interaction, thereby creating a momentum unbalance similar to that in events with antineutrons; 2 - in our energy $2E_b < 2$ GeV the speed of K_L can be considerably lower than speed of light, therefore the signal from them is delayed as for antineutrons. The measured residual cosmic background rate has the intensity ~ 0.01 Hz, which corresponds to the suppression of the number of cosmic events, that have pass the hardware selection in the detector electronics, approximately by 2×10^4 times.

The numbers $N_{n\bar{n}}$ of found events are listed in the Table I with the total number close to 8000. The Table shows only statistical errors of the fitting in $N_{n\bar{n}}$. A sources of systematic error in the $N_{n\bar{n}}$ number can be uncertainties in the magnitude and shape of the time spectrum of the beam and cosmic background. The error introduced by these sources is about

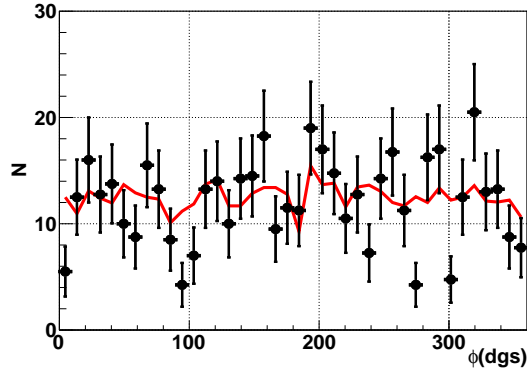


FIG. 4: The antineutron azimuthal angle distribution for data (points with error bars) and MC (horizontal line) at $E_b = 953$ MeV.

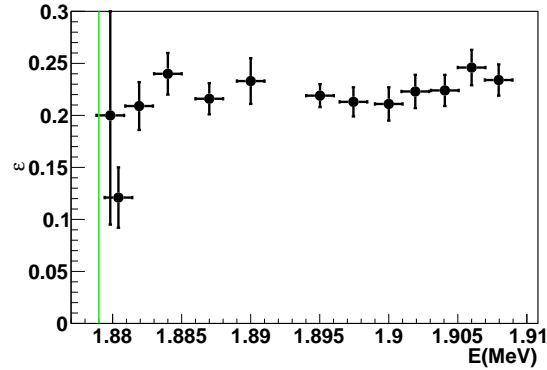


FIG. 6: The corrected MC detection efficiency versus energy. Vertical line corresponds to $n\bar{n}$ threshold.

10 events what is much lower than statistical errors in the Table I and is not taken into account in what follows.

IV. ANGULAR DISTRIBUTION

The antineutron production angles θ_n and ϕ_n , as it mentioned in Section II, are determined by the direction of the event momentum. The accuracy of the antineutron angle measurement was determined by MC simulation by comparing the true angle and the angle

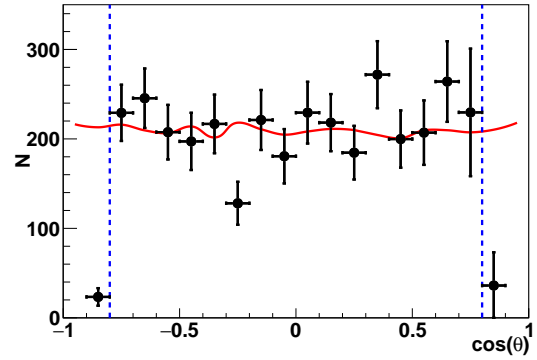


FIG. 5: The antineutron polar angle distribution for data (points with error bars) and MC (horizontal line) at $E_b = 940$ MeV. Dotted vertical lines correspond to the polar angle cutoff.

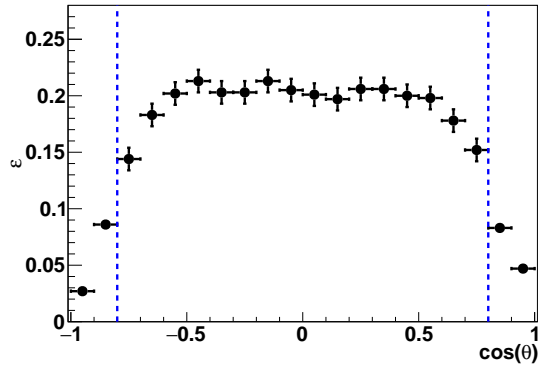


FIG. 7: The MC detection efficiency as a function of antineutron $\cos \theta$ at $E_b=940$ MeV. Dotted vertical lines correspond to the polar angle cutoff.

calculated from the direction of the event momentum. The angular accuracy turned out to be about 6 degrees, which is somewhat less than the angular size of one calorimeter crystal (9 degrees).

The distribution of the selected data and MC simulated $n\bar{n}$ events over azimuthal angle ϕ_n (Fig. 4) is uniform as expected, what confirms the correct subtraction of the beam and cosmic backgrounds, which are not uniform over ϕ_n angle. Distribution over $\cos\theta_n$ for data and MC events is shown in Fig. 5. The MC simulation was done using Eq. (1) with the assumption $|G_E| = |G_M|$. Since we are working in the immediate vicinity of the threshold, the condition $|G_E| \simeq |G_M|$ is required. In our case of spherical shape of the SND calorimeter, the data distribution over $\cos\theta_n$ is expected to be close to uniform, and this is confirmed in Fig. 5.

V. DETECTION EFFICIENCY

The $e^+e^- \rightarrow n\bar{n}$ process detection efficiency ε in different energy points under accepted selection conditions (Section II) is shown in Fig. 6. When simulating the detector response we used the MC GEANT4 toolkit [12], version 10.5. The angular distribution of produced $n\bar{n}$ pairs corresponded to $|G_E|/|G_M|=1$, The simulation included the beam energy spread ~ 0.7 MeV and the emission of photons by initial electrons and positrons. The simulation also took into account non-operating detector channels as well as overlaps of the beam background with recorded events. To do this, during the experiment, with a pulse generator, synchronized with the moment of beam collision, special superposition events were recorded, which were subsequently superimposed on MC events. The detection efficiency ε in Fig. 6 is corrected for the difference between the data and MC. This correction is discussed later. Numerical values of the efficiency are given in the Table I. In Fig. 7 the detection efficiency versus $\cos\theta$ of antineutron is shown.

The detection efficiency in our measurement is of order of 20%, what is insufficient for such a complex process to analyze as $e^+e^- \rightarrow n\bar{n}$. In the list of selection conditions (chapter II), the greatest contribution to the loss of efficiency is made by the cosmic background suppression parameter $shcosm$ (number 6 in the list), where the loss of efficiency is about 50%. All other selection conditions result in a significantly smaller efficiency loss $\sim 1-20\%$ for each. For correct calculation of efficiency in general, it is important to find out how correctly

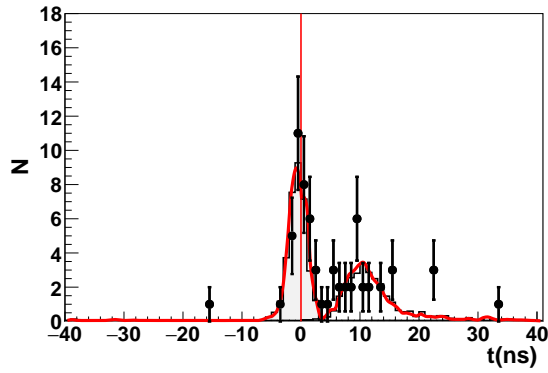


FIG. 8: The event time spectrum with tracks in drift chamber at $E_b=943.5$ MeV. The peak at $t=0$ corresponds to the beam and physical background. The wide peak from the right is the $n\bar{n}$ signal.

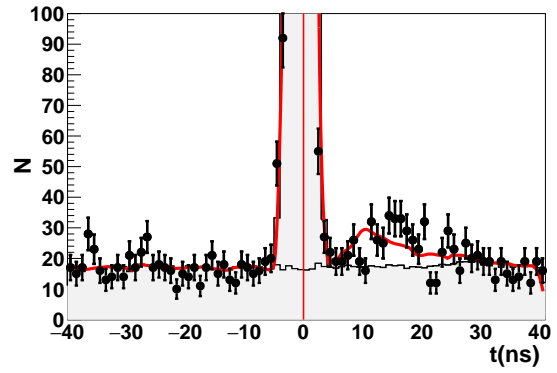


FIG. 9: The event time spectrum with inverted EMC energy cut $E_{EMC} < E_b$. The peak at $t=0$ corresponds to the beam and physical background. The wide peak from the right is the delayed $n\bar{n}$ signal.

the proportion of events outside the selection condition is simulated. To do this, we invert the selection conditions for each selection condition or a pair of related conditions and then calculate the corresponding corrections δ for detection efficiency in each of 13 energy points as follows:

$$\delta = \frac{n_0}{n_0 + n_1} \frac{m_0 + m_1}{m_0}, \quad (5)$$

where n_0 (n_1) is the number of $n\bar{n}$ data events determined with standard (inverted) selection cuts. These numbers were calculated during the time spectra fitting with the Eq.4, as it is described in the chapter III. The values m_0 and m_1 refer respectively to the MC simulation event numbers. Examples of the time spectra obtained with inverted conditions are shown in Figs. 8, 9.

Below we will give some comments on obtaining correction factors δ for detection efficiency. During the initial selection of events for $n\bar{n}$ analysis, events with tracks not from the interaction region are allowed. The condition for such tracks is $D_{xy} > 0.5$ cm, where D_{xy} is the distance between the track and the axis of the beams. Accordingly, the events with $D_{xy} < 0.5$ are rejected. There is no significant loss of $n\bar{n}$ events due to this conditions. On the other side, the events of the beam and physical background, with tracks predominantly from the beam region, are strongly suppressed. When inverting the selection condition on the number of charged tracks ($n_{ch}>0$), it is worth to consider the possible background from

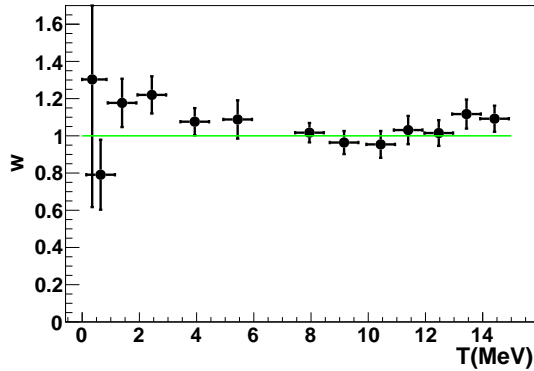


FIG. 10: The total detection efficiency correction, obtained using Eq.6, versus antineutron kinetic energy $T = E_b - m_n$. Horizontal line corresponds to no correction case.

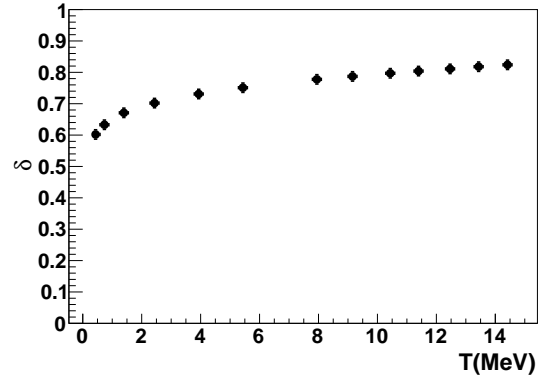


FIG. 11: The radiative correction to the $e^+e^- \rightarrow n\bar{n}$ process as a function of kinetic energy $T = E_b - m_n$.

the related process $e^+e^- \rightarrow p\bar{p}$. In this experiment at the beam energy $E_b < 955$ MeV the protons and antiprotons are slow and stop in the collider vacuum pipe. Here the antiproton annihilates with the production of charged tracks, most of which have $D_{xy} > 0.5$ cm and are included in the inverse selection $n_{ch} > 0$. But even such a background from the $e^+e^- \rightarrow p\bar{p}$ will be suppressed when fitting the time spectrum, since it practically merges in time with the beam background. An example of a time spectrum with inverse selection condition $n_{ch} > 0$ is shown in Fig. 8.

To study the effect of the energy threshold in the EMC, the inverse condition $0.7E_b < E_{cal} < E_b$ is applied. An example of time spectrum under this condition is shown in Fig. 9. Here, in contrast to Fig. 8, a sharply increased beam and cosmic background is seen. However, the $n\bar{n}$ signal is clearly visible here too, which makes it possible to calculate the efficiency correction.

An additional correction arises from the events with EMC energy $E_{cal} < 0.7E_b$. These events are not recorded in the Ntuples for analysis due to the large background. In events with such low EMC energy antineutron is absorbed usually in the 3-d calorimeter layer or outside the calorimeter. Fortunately, the proportion of such events is small: 3.5% at $E_b=954$ MeV and 1% at $E_b=940$ MeV. Monte Carlo studies show that these events are solely represented by the contribution of the antineutron scattering process. It was previously noted in chapter III, that to describe the shape of data time spectrum the contribution of

the process of antineutron scattering in MC should be reduced by a factor of 1.5-2. With such a change, the proportion of events with $E_{\text{cal}} < 0.7E_b$ in MC reduces to 0.7% at $E_b=940$ MeV and to 2% at $E_b=954$ MeV. The difference between the initial and modified values is taken as an error to the final correction. The sign of this correction is positive, it increases the detection efficiency by several percent.

Next, we calculated the corrections to the detection efficiency for all selection conditions (chapter II) using Eq.5. Then, considering the corrections to be uncorrelated, we calculate the total correction for a given energy as:

$$\delta_{\text{tot}} = \prod(1 + \delta_i) - 1. \quad (6)$$

Its energy dependence shown in Fig. 10. It can be seen, that if we exclude two energy points near the threshold, the total correction increases the $e^+e^- \rightarrow n\bar{n}$ process detection efficiency by $\sim 10\%$. The corrected detection efficiency is obtained from the MC efficiency by multiplying by the total correction δ_{tot} . The values of the corrected efficiency are given along with systematic errors in the Table I and shown in Fig. 6.

VI. THE MEASURED $e^+e^- \rightarrow n\bar{n}$ CROSS SECTION

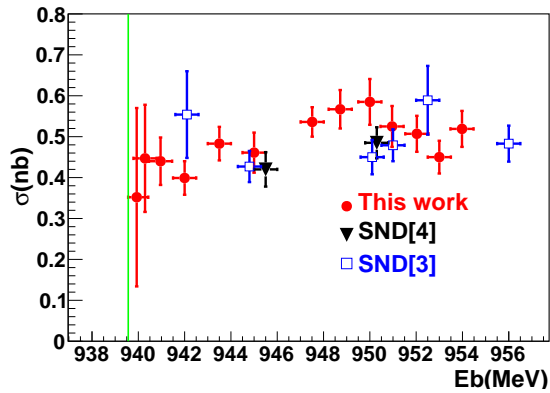


FIG. 12: The measured $e^+e^- \rightarrow n\bar{n}$ cross section in the vicinity of the nucleon threshold. The vertical line is the $n\bar{n}$ threshold.

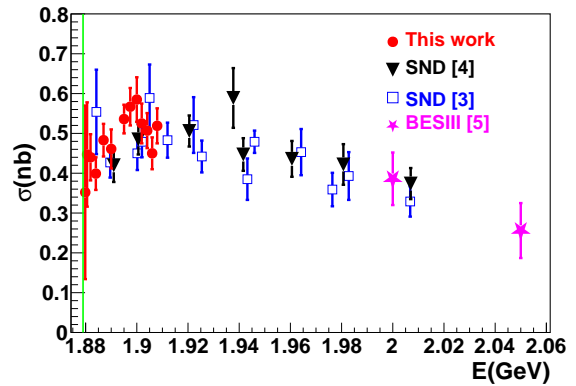


FIG. 13: The measured $e^+e^- \rightarrow n\bar{n}$ cross section as a function of neutron momentum in comparison with previous measurements. The vertical line is the $n\bar{n}$ threshold.

Using the number of $n\bar{n}$ events $N_{n\bar{n}}$, luminosity L and detection efficiency ε (Table I), the visible cross section $\sigma_{\text{vis}}(E) = N_{n\bar{n}}/L\varepsilon$ can be calculated. The Born cross section $\sigma(E)$,

that we need, is related to the visible cross $\sigma_{vis}(E)$ in the following form :

$$\begin{aligned}\sigma_{vis}(E) &= \sigma(E)(1 + \delta(E)) \\ &= \int_{-\infty}^{+\infty} G(E', E)dE' \\ &\quad \int_0^{x_{max}} W(s, x)\sigma(s(1 - x))dx,\end{aligned}\tag{7}$$

where $W(s, x)$ is the radiator function [13], describing emission of photons with energy $x E_b$ by initial electrons and positrons, $G(E', E)$ is a Gaussian function describing the c.m. energy spread. In function $W(s, x)$ the contribution of the vacuum polarization is not taken into account, so our Born cross section is the “dressed” cross section. The factor $(1 + \delta(E))$ takes into account both the radiative corrections and beam energy spread. This factor (Fig.11) is calculated in each of 13 energy points using the Born cross section, obtained by the fitting of the visible cross section using Eq. 7. The energy dependence of the Born cross section is described by Eq.2, in which the form factor is a 2-nd order polynomial of the neutron momentum. The parameters of this polynomial were free fit parameters. The resulting Born cross section is shown in the Figs. 12, 13 as a function of the neutron energy and momentum. Numerical values of the cross section are given in the Table I. The dominant contribution into systematic error in the measured cross section is made by the detection efficiency correction error, In this error the uncertainties in the value of luminosity (2%) and radiative correction (2%) are also taken into account. In Figs. 12, 13 the total statistical and systematic error is shown. In comparison with previous SND measurements [3], [4], this paper presents data in the immediate vicinity of the $n\bar{n}$ threshold. At the beam energy points of 942, 945 and 950 MeV, the obtained cross section agrees with the previous SND results At energy points extremely close to the threshold (939.6, 940.2 MeV) the measured cross section does not drop to zero and is approximately 2 times lower than the $e^+e^- \rightarrow p\bar{p}$ cross section [14],[15].

VII. THE NEUTRON EFFECTIVE TIMELIKE FORMFACTOR

The effective neutron form factor calculated from the measured cross section using Eq. (2) is listed in the Table I and shown in Fig. 14 as a function of the antineutron energy and in Fig. 15 as a function of the antineutron momentum. The results of previous measurements are also shown. For comparison the Fig. 14 shows the proton form factor measured in the

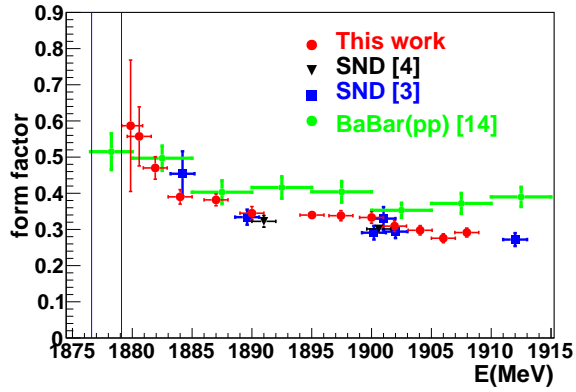


FIG. 14: The measured effective neutron timelike form factor in the vicinity of the nucleon threshold. For comparison the proton form factor measured in the Babar experiment [14] is shown. Vertical lines correspond to the position of the proton and neutron-threshold.

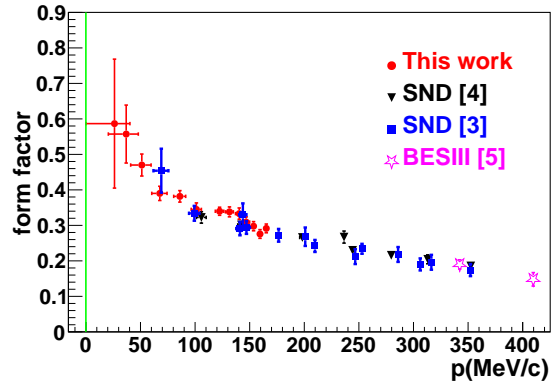


FIG. 15: The measured effective neutron timelike form factor as a function of neutron momentum, compared with previous measurements.

Babar experiment [14],[15]. It is seen that closer to the threshold the neutron formfactor value is about 0.6 and the form factors of the neutron and proton approach each other, although the error in the measurement of neutrons is still large $\sim 30\%$. Most predictions of nucleon form factors values refer to the asymptotic region of large momentum transfers, there is no unambiguous prediction for our case of the threshold region.

VIII. SUMMARY

The experiment to measure the $e^+e^- \rightarrow n\bar{n}$ cross section and the neutron timelike form factor has been carried out with the SND detector at the VEPP-2000 e^+e^- collider at energies in c.m. from the process threshold to 1908 MeV. The measured cross section varies with energy within $0.4 \div 0.6$ nb. At the energy point closest to the threshold, the cross section is about 0.4 nb. There are no contradictions with previous SND measurements. The neutron effective timelike form factor, extracted from the measured cross section, shows an increase to a value of 0.6 at the very threshold. A tendency is visible for the form factors of the neutron and proton to converge at the threshold.

ACKNOWLEDGEMENTS. This work was carried out on the Russian Science Foundation grant No. 23-22-00011.

- [1] A. Antonelli *et al.* (FENICE Collaboration), Nucl. Phys. B **17**, 3 (1998), [https://doi.org/10.1016/S0550-3213\(98\)00083-2](https://doi.org/10.1016/S0550-3213(98)00083-2)
- [2] M.F. Biagini *et al.* (DM2 Collaboration), Z. Phys. C **52**, 631 (1991), <https://doi.org/10.1007/BF01562337>
- [3] M. N. Achasov *et al.* (SND Collaboration), Eur. Phys. J. C (2022:82:761). <http://doi.org/10.1140/epjc/s10052-022-10696-0>
- [4] M. N. Achasov *et al.* (SND Collaboration), Phys. Atomic Nucl. **86** No.6, 937 (2023), <http://doi.org/10.134/S1063778823060054>
- [5] M. Ablikim *et al.* (BESIII Collaboration), Nat. Phys. **17**, 1200 (2021). <https://doi.org/10.1038/s41567-021-01345-6>
- [6] P. Yu. Shatunov *et al.*, Part. Nucl. Lett. **13**, 995 (2016). <http://dx.doi.org/10.1134/S154747711607044X>
- [7] M. N. Achasov *et al.* (SND Collaboration), Nucl. Instrum. Meth. A **449**, 125 (2000). [http://dx.doi.org/10.1016/S0168-9002\(99\)01302-9](http://dx.doi.org/10.1016/S0168-9002(99)01302-9)
- [8] M. Astrua *et al.*, Nucl. Phys. A **697**, 209 (2002). [http://dx.doi.org/10.1016/S0375-9474\(01\)01252-0](http://dx.doi.org/10.1016/S0375-9474(01)01252-0)
- [9] M. N. Achasov *et al.*, JINST **10**, T06002 (2015). <http://dx.doi.org/10.1088/1748-0221/10/06/T06002>
- [10] M. N. Achasov *et al.*, Nucl. Instrum. Meth. A **1056**, 168664 (2023). <http://dx.doi.org/10.1016/j.nima.2023.168664>
- [11] A. V. Bozhenok *et al.*, Nucl. Instr. Meth. A **379**, 507 (1996). [http://dx.doi.org/10.1016/0168-9002\(96\)00548-7](http://dx.doi.org/10.1016/0168-9002(96)00548-7)
- [12] J. Allison *et al.* (GEANT Collaboration), Nucl. Instr. Meth. A **835**, 186 (2016). <https://doi.org/10.1016/j.nima.2016.06.125>, <https://geant4-data.web.cern.ch/-ReleaseNotes/ReleaseNotes4.10.5.html>
- [13] E. A. Kuraev and V. S. Fadin, Sov. J. Nucl. Phys. **41**, 466 (1985).
- [14] J. P. Lees *et al.* (BABAR Collaboration), Phys. Rev. D **87**, 092005 (2013).

<http://dx.doi.org/10.1103/PhysRevD.87.092005>.

- [15] J. P. Lees *et al.* (BABAR Collaboration), *Phys. Rev. D* **88**, 072009 (2013).

<http://dx.doi.org/10.1103/PhysRevD.88.072009>.